Journal of Alloys and Compounds 670 (2016) 188–197

Contents lists available at ScienceDirect

Journal of Alloys and Compounds

journal homepage: http://www.elsevier.com/locate/jalcom

Effect of Ni addition on the contact resistance of Ag-WC electrical contacts

Nachiketa Ray [a, *], Bernd Kempf [b], Timo Mützel [b], Frank Heringhaus [b], Ludo Froyen [a], Kim Vanmeensel [a], Jef Vleugels [a]

[a] Department of Materials Engineering, KU Leuven, Kasteelpark Arenberg, 44, 3001 Leuven, Belgium
[b] Umicore AG & Co. KG, Rodenbacher Chaussee 4, 63457 Hanau-Wolfgang, Germany

ARTICLE INFO

Article history:
Received 9 September 2015
Received in revised form
1 February 2016
Accepted 4 February 2016
Available online 16 February 2016

Keywords:
Metal matrix composites
Powder metallurgy
Phase diagrams
Scanning electron microscopy

ABSTRACT

In this work, Ni was used as an additive in Ag-WC (60–40 wt.%) metal matrix composites employed as electrical contacts. Increasing the Ni content from 1 to 3 wt.% resulted in an increase in the mean electrical contact resistance (R_c) from ~2 to ~3 mΩ. However, further addition of Ni up to 10 wt.% resulted in the formation of a silver layer on the contact surface after switching, which strongly reduced the R_c from ~3 to ~1.5 mΩ. The influence of Ni addition on the microstructural changes in the contact material was investigated and the mechanism for the transfer of silver from the bulk composite material to the surface as a consequence of thermal cycling during switching was elucidated.

1. Introduction

In the electrical industry, low-voltage circuit breakers have been using silver based metal matrix composites (MMCs) [1–6] due to their superior electrical, thermal and oxidation properties compared to copper. The secondary phase in the metal matrix is usually a refractory metal or carbide, which minimizes the arc-erosion/mass loss [5,7–9] and prevents the contacts to weld together at overrated currents (short circuit current) [3,10–12]. Although addition of the refractory phase improves the arc-erosion properties, it increases the electrical contact resistance (R_c) of the composite. Thus depending on the application, the volume fraction of silver is adjusted accordingly to regulate the R_c of the composite, which is essential to limit the temperature rise inside the device. Thus in most cases, Ag-WC contact materials consist of a large volume fraction of silver which forms a ductile and percolating network of metal matrix to maintain a low R_c. Alternative methods of regulating R_c have been of substantial interest which include, manipulating the composition of the composite by adding dopants [13–16] and by modifying the microstructure [17,18].

Transition metals like Ni and Co are well known binders for sintering of W and WC in cermets [19–22] and as a wetting agent for silver–carbon interfaces [23]. The influence of Ni in Ag–W/WC contact materials has been studied in the past and the effect of Ni on the R_c [13,14,24] and arc-erosion [15] has been of significant interest. The rise in R_c for these materials has been associated with the formation of tungsten oxides and nickel tungstates [13], but the influence of Ni on the R_c is still not clear. In this work, a more fundamental approach has been pursued to study the composites after switching and correlate the microstructure with thermodynamic equilibrium phase diagrams to elucidate the influence of Ni addition in Ag-WC contact materials.

2. Experimental approach

2.1. Densification by liquid metal infiltration

Pellets with a diameter of 7 mm were produced via powder metallurgical route in which, a powder mixture of Ag (d_{50}~5 μm), WC (d_{50}~0.8 μm), and Ni (d_{50}~7 μm) was pre-compacted by uniaxial pressing and sintered to form a porous network, which was later densified by molten silver infiltration. Different starting

* Corresponding author.
E-mail addresses: nachiketa.ray@mtm.kuleuven.be, nachiketa.ray.1014@gmail.com (N. Ray).

http://dx.doi.org/10.1016/j.jallcom.2016.02.037
0925-8388/

powder compositions were necessary for achieving different final composite compositions. For preparing an electrical contact with 60 wt.% Ag, 33.5 wt.% WC and 6.5 wt.% Ni the following process was followed. A starting powder containing a mixture of 40 wt.% Ag, 51 wt.% WC and 9 wt.% Ni was pressed to a pre-defined density so that the composite achieved the final desired composition after sintering and silver infiltration. Sintering was carried out at 970 °C for 30 min and infiltration at 1070 °C for 30 min, i.e. above the liquidus of silver, in a reducing atmosphere containing a mixture of hydrogen and nitrogen (3:1) in order to prevent oxidation of the tungsten carbide. A graphite crucible was used to place the pellets in the furnace for both sintering and infiltration, since silver does not wet graphite. Ni1Ag56, Ni3Ag58, Ni6.5Ag57 and Ni10Ag55 compositions, reflecting the overall wt.% Ni and Ag content (balanced by WC), were prepared and investigated, corresponding to a vol.% composition of Ni1.4Ag65, Ni4Ag66, Ni8.6Ag64 and Ni13Ag61 respectively. Backscattered electron micrographs of the infiltrated Ag-WC-Ni composites are shown in Fig. 1. The microstructures appear to be dense and consist of three phases viz. WC (bright), Ag (dark) and Ni (black). Table 1 summarizes the four Ag-WC-Ni contact materials along with their starting powder compositions and final compositions. The densities of the pellets were measured using the Archimedes' principle in water and are tabulated in Table 1. The measurements confirm that the composites achieved near theoretical density (~99%) after infiltration.

The Vickers hardness of the Ag-WC-Ni composites was measured (Model FV-700, Future-Tech Corp., Tokyo, Japan) with a load of 0.5 kgf and a dwell time of 15 s Table 1 shows the evolution of the hardness as a function of the Ni content. It clearly shows that the hardness decreases with increasing ductile phase content (Ag + Ni) in the composites. A previous study [17] revealed that the R_c of the composite would decrease monotonously with increasing ductility of the composite, unless some additional factors like phase transformation influence the microstructure.

2.2. Break-only model switch and measurement of electrical contact resistance (R_c)

The dense disc shaped composites were brazed to a copper rod (Ø = 8 mm, 45 mm high) and successively turned down to a diameter of 4 mm and height of 2 mm to yield a flat contact surface (Fig. 3 (a)). Two identical composites were tested as a contact pair in a break-only model switch [3,17]. In this device a contact pair was brought together and a half sinusoidal current wave, having a frequency of 50 Hz and peak current of 1300 A was applied. Then the contacts were opened at the beginning of the sinusoidal current (i = 0), during which the current flowed for one half-cycle to observe an electric arc until next current zero. After the arc had been extinguished completely by a thyristor, the contacts were re-closed for electrical contact resistance (R_c) measurement, during which the voltage drop across the contacts was measured using a direct current of 10 A. This procedure was carried out for 50 cycles and the electrical contact resistance (R_c) was measured after each cycle. This test was inspired by the standard Sequence X of U.L. 489 [25]. The arcing contacts studied in this context usually find application in low voltage and high current miniature circuit breakers (MCB) and molded case circuit breakers (MCCB).

2.3. Characterization

The post-switching surface was characterized using a confocal scanning laser microscope. The contact surface was also analyzed by X-ray diffraction (XRD, 3003-TT, Seifert, Ahrensburg, Germany) using Cu K_α radiation at 40 kV and 40 mA. XRD patterns were recorded by θ–2θ mode with a scan speed of 2s/step and a scan size of 0.02°. The transverse section of the composite was investigated for microstructural characterization, i.e., the plane perpendicular to the contact surface. The plane of interest was sectioned using a low speed diamond saw and appropriate metallographic sample

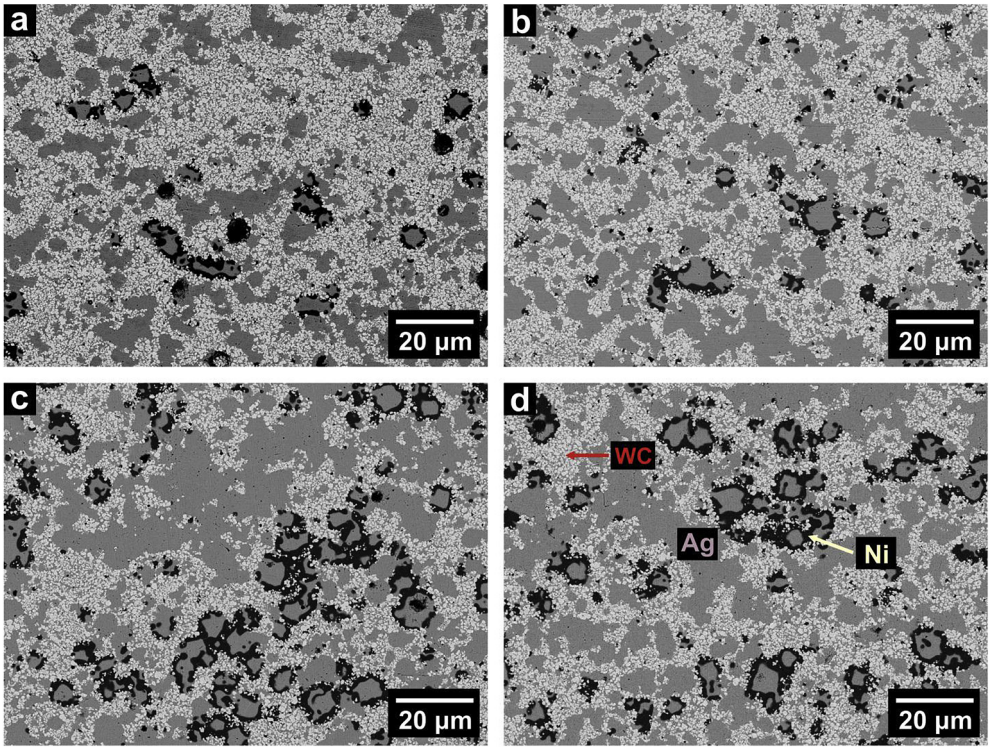

Fig. 1. Backscattered electron micrographs of the infiltrated Ag-WC-Ni materials before switching. (a) Ni1Ag56, (b) Ni3Ag58, (c) Ni6.5Ag57 and (d) Ni10Ag55.

Table 1
Ag-WC-Ni contacts (see Fig. 1) investigated in this work, tabulating their starting powder composition, final composition after infiltration (balance WC), density and Vickers hardness.

Contact material	Powder composition		Final composition		Density ($g \cdot cm^{-3}$)	Relative TD (%)	Vickers hardness ($HV_{0.5}$)
	Ag (wt.%)	Ni (wt.%)	Ag (wt.%)	Ni (wt.%)			
a	40	1.5	56	1	12.15	99.68%	218.3 ± 2.5
b	40	4.5	58	3	11.83	98.91%	208.5 ± 0.8
c	40	9.0	57	6.5	11.64	98.94%	199.1 ± 2.1
d	40	13.5	55	10	11.55	99.36%	182.3 ± 1.5

preparation was carried out as mentioned in Ref. [17]. Scanning electron microscopy (XL 30 FEG, FEI) was used for investigating the initial and post-switching microstructures. Elemental mapping and quantitative elemental analysis were performed using Electron probe micro-analysis (EPMA, JXA-8530F, JEOL). Equilibrium phase diagrams were calculated to examine the stability of the phases formed after switching, based on elemental analysis using Thermo-Calc-4.0 software.

3. Results

The surface of the contact pair after 50 switching operations is shown in Fig. 2. The materials with low Ni content have a darker (oxidized) surface than the ones with the higher Ni content. For materials containing more than 6.5 wt.% Ni, the surface contained pools of shiny non-oxidized metal. The evolution of the measured electrical contact resistance (R_c) during 50 switching cycles is plotted in Fig. 3 (b). The plot shows that the R_c builds up to 20 switching cycles for most cases and then reaches a stable value. The graph clearly indicates that the R_c plateau value decreases with increasing amount of Ni in the material (3–10 wt.%).

During each switching operation, the electric arc strikes the contact surface and severely degrades the material. Such deterioration is manifested by material loss, thermal stress induced cracking [17,26,27], microstructural changes and oxidation, where material loss is a direct consequence of the vaporization and splash erosion of silver [28]. Metallographic investigation of the cross-sectioned materials after switching revealed a different microstructure depending on the Ni content of the composite. Even though Ni and Ag share the same crystal structure, similar electronegativity and small difference in atomic radii (<15%), they have a limited solubility in both solid and liquid state due to a large positive enthalpy of mixing [29]. Therefore, Ag, WC and Ni are present as separate phases in the pristine materials as shown in Fig. 1. Here Ni was identified to mainly segregate around the silver phase in the bulk material. For materials having very low Ni content (~0.1 wt.%), the microstructure of the "arc-affected zone" was similar to the bulk but contained a lot of cracks [17]. However, for high Ni containing materials the "arc-affected zone" showed a distinctly different microstructure compared to the bulk.

Fig. 4 and Fig. 5 illustrate the elemental distribution in the transverse section of the lower arced contacts of all four Ni containing Ag-WC materials, measured using EPMA wavelength dispersive spectroscopy. The micrographs can be clearly classified into an "arc-affected zone" and bulk region. The arc-affected zone can be further divided into two or three distinct layers. The top layer (marked as region i in Fig. 5) consists of a very thin silver-rich layer with a small amount of segregated Ni (Fig. 6 (a)). This layer explains the shiny non-oxidized metallic surface in Fig. 2 (c, d). This layer is only present in the contact material containing 6.5 and 10 wt.% of Ni. A similar Ag layer formation on top of the contact surface was also reported for Ag–12Ni electrical contacts even after 50000 dc switching operations [30]. The second layer from the top (region ii in Fig. 4 and Fig. 5) is a silver-free layer consisting of large faceted WC grains, which are sintered together with a Ni-rich eutectic phase. At higher magnification, the lathes of the eutectic were clearly visible (Fig. 6 (b)). The distance between the lathes was around ~50 nm. The third layer (region iii in Fig. 4 and Fig. 5) is a Ni-depleted region, which mainly consists of smaller and faceted grains of WC and silver. This region still contains some Ni, but less

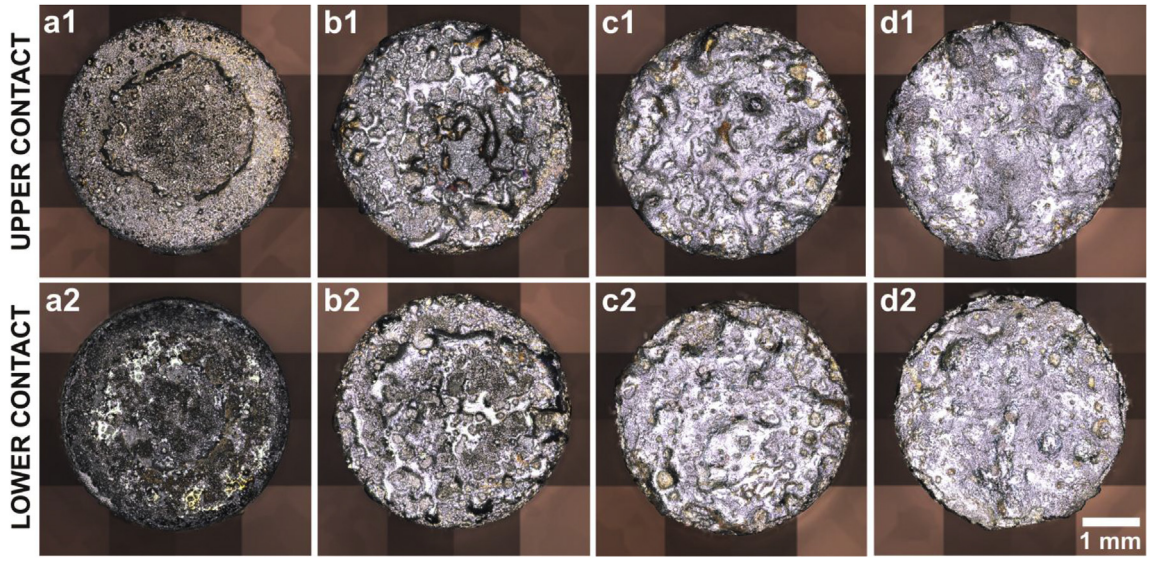

Fig. 2. Upper and lower contact surface of (a) Ni1Ag56, (b) Ni3Ag58, (c) Ni6.5Ag57 and (d) Ni10Ag55 (wt.%) contact materials after 50 switching cycles.

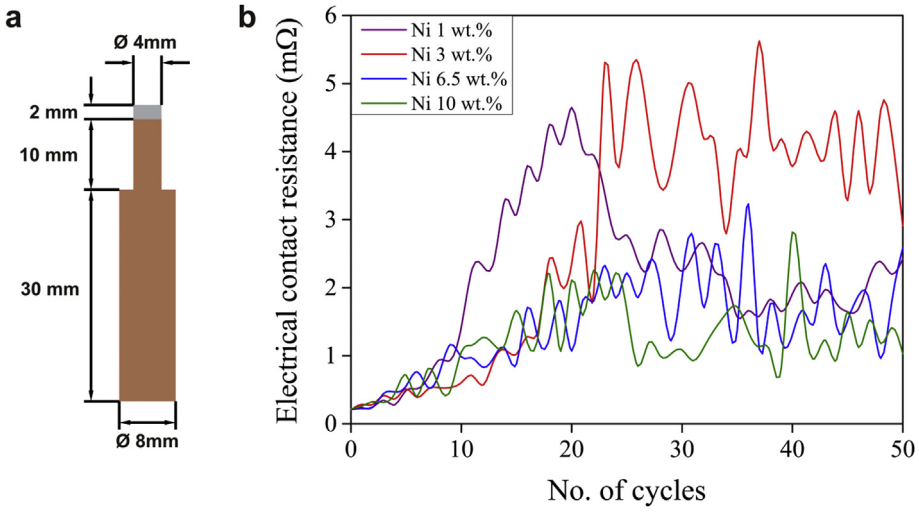

Fig. 3. (a) Dimensions of the contact piece (grey) brazed to the copper rod used in the break-only model switch. (b) Evolution of the electrical contact resistance (R_c) over 50 switching cycles as a function of Ni content.

compared to the bulk material below this layer.

Fig. 6 specifically illustrates the elemental distribution in the transverse section of the lower arced contact containing 10 wt.% of Ni which is the most interesting case since it showed the lowest contact resistance. Thus for this case the average elemental intensities in the profiles were calculated along a horizontal line parallel to the surface and normalized on an identical scale for Ag, W and Ni. This average normalized intensity was plotted as a function of distance from the contact surface as shown in Fig. 5 (b). The plot was further smoothened using a Savitzy-Golay filter which minimized the signal-to-noise ratio using local 2nd order polynomial fitting. This plot illustrates the Ag-rich, Ag-depleted and Ni-depleted layers as a function of depth from the contact surface.

The appearance of the silver layer with increasing Ni content is consistent with the phase evolution within the silver-depleted layer, which is shown in Fig. 7. Three distinct phases (1, 2 and 3) can be differentiated in the micrographs, which were quantitatively analyzed using wavelength dispersive X-ray spectroscopy. The elemental analysis tabulated in Table 2 reveals that the large polygonal dark grains (Phase 1) are stoichiometric WC crystals and the rounded bright grains (Phase 2) are non-stoichiometric tungsten rich carbide ($W_2C_{1-x}Ni_x$) with Ni in solid solution. Their rounded shape is due to activated sintering in the presence of Ni [19,31] which leads to de-faceted grain boundaries in contrast to the faceted surfaces in case of sintered WC. It is important to observe that the dark eutectic phase (Phase 3) in-between the large WC grains grew at the expense of the rounded bright grains with increasing Ni content. The eutectic phase is completely absent in the material containing only 1 wt.% of Ni (Fig. 7 (a)), whereas it replaces most of the bright grains (Phase 2) in the material containing 10 wt.% of Ni (Fig. 7 (d)). Thus the volume fraction of the eutectic phase in the silver depleted layer can play a role in the formation of the silver surface layer which increases with increasing Ni content. The average depth of these layers present in the contacts after 50 switching cycles was measured from the micrographs at 10 different positions on each contact and is plotted in Fig. 8 (a). It is important to note that the constituent layers were continuous for the material containing 6.5 and 10 wt.% of Ni, whereas the silver depleted layer was interrupted in the lower Ni content materials, (Fig. 4 (a)). This is mainly because the ductility of these layers changes as a function of the Ni content. With increasing Ni content the dark eutectic phase replaces the brittle $W_2C_{1-x}Ni_x$ which leads to a more ductile and continuous layer formation during switching. Although the absolute thickness of each layer does not correlate with the R_c, the volume fraction of each phase in the layers are important. The top silver layer which was only present in the material containing 6.5 and 10 wt.% of Ni, was discontinuous and thinner in the 6.5 wt.% Ni material and continuous and thicker in the 10 wt.% Ni grade. However, only two dimensional sections were observed in this study thus stereological factors must also be considered.

To examine the homogeneity of the surface layers formed after switching, X-ray diffraction studies were carried out on the surface of the lower contact and compared with microstructural analysis. Fig. 8 (b) shows the XRD patterns recorded in the range of 30–55° (2θ) for the four investigated contact materials containing 1, 3, 6.5 and 10 wt.% of Ni. It is important to note that the interaction volume of the X-rays is limited to the silver layer and silver depleted layer (Fig. 8 (a)) for a material rich in WC which has a very high absorption coefficient for X-rays. The graph reveals that the amount of silver increases with increasing Ni content, which is an outcome of the silver layer formation as observed in the elemental analysis. $Ni_{17}W_3$ (PDF no. 03-065-4828) [32] was also detected in the XRD pattern and it evolves with increasing Ni content, but was absent in the 1 wt.% Ni grade. As recognized from the elemental analysis and microstructural investigation, this Ni rich phase (phase 3 in Fig. 7) grows at the expense of the W_2C with increasing Ni content, which is also confirmed by the XRD patterns. A small amount of Ni (~1 wt.%) in the contact material leads to carbon depletion of the WC during switching leading to the formation of metastable W_2C and sometimes also a tungsten oxycarbide (W_2CO) (PDF no. 00-022-0959) [33] which is a result of the interaction of tungsten oxide vapor with free carbon at high temperatures.

To understand the formation of these layers as a result of switching, the thermodynamic stability of the phases had to be determined. Thermodynamic equilibrium diagrams are useful to predict and investigate all possible phase transformations in a given system. However, the temperatures and compositions which are applicable in this condition should be known. Theoretically, the temperature of the contact should be limited to the boiling point of silver (2160 °C), as long as silver is available in the bulk due to the latent heat of vaporization. Yet local rises in surface temperature lead to melting of WC (2785 °C) which was observed in the present study and also in materials having very low Ni content (~0.1 wt.%)

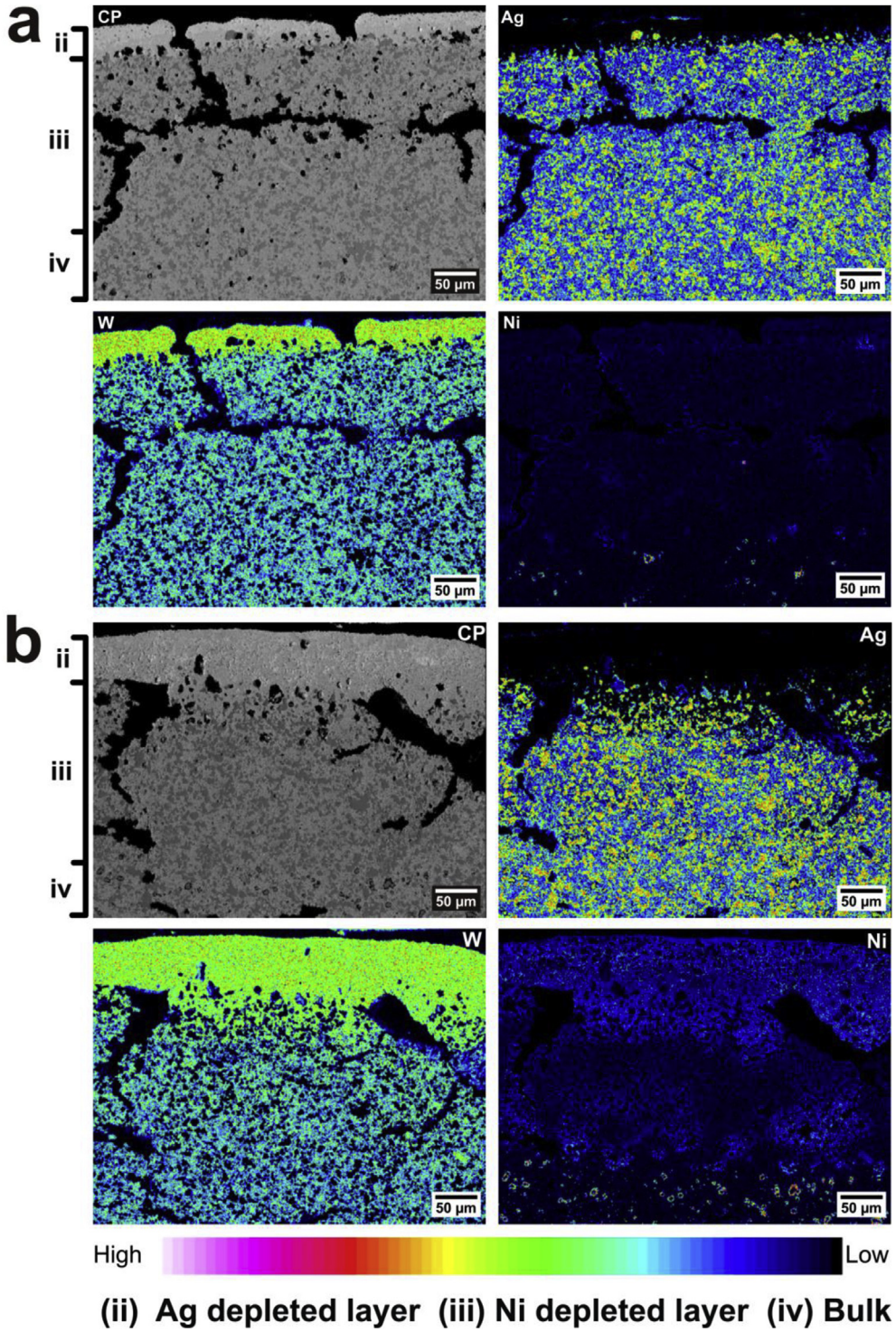

Fig. 4. EPMA wavelength-dispersive X-ray spectroscopy elemental mapping of the transverse section of the lower contact of (a) Ni1Ag56 and (b) Ni3Ag58 material after 50 switching cycles (Fig. 2 (a2 and b2)); the map shows the distribution of Ag, W and Ni and clearly demarcates the different layers of the 'arc affected zone' (the Ag depleted and Ni depleted layer) from the bulk.

[17]. This gives an empirical knowledge of the surface temperatures of the contacts during arcing.

Elemental W and Ni are known to form a eutectic at 1495 °C [34,35], and a more stable intermetallic Ni_4W is formed around 1000 °C. However, switching at overrated currents is a very rapid heating and cooling cycle which may prevent the formation of equilibrium phases. Thus the liquid phase which is Ni-rich in the WC-Ni phase diagram [21] (i.e. the hypoeutectic region) is quenched, forming an eutectic composed of WC (bright dispersed eutectic phase in Fig. 6(b) and Fig. 7(d)) and a solid solution (fcc) of WC in Ni (dark eutectic matrix phase in Fig. 7(d)). The composition of the eutectic phase plays an important role to study the equilibrium phase diagrams and was thus measured (Table 2).

Although Ag and Ni have limited solubility in the solid and

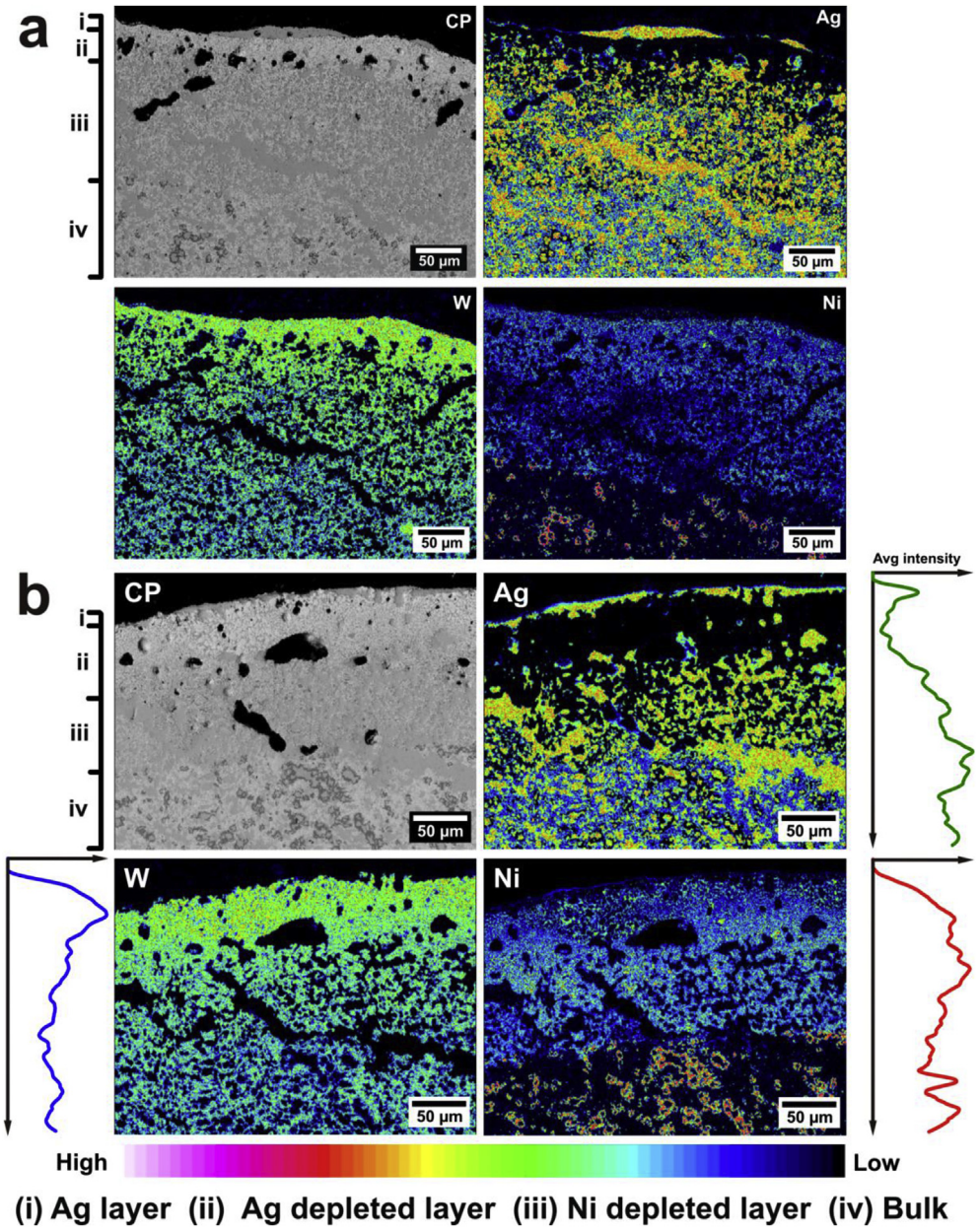

Fig. 5. EPMA wavelength-dispersive X-ray spectroscopy elemental mapping of the transverse section of the lower contact of (a) Ni6.5Ag57 and (b) Ni10Ag55 material after 50 switching cycles (Fig. 2 (c2 and d2)); the map shows the distribution of Ag, W and Ni and the elemental intensity profiles represent the averaged line intensities parallel to the surface.

liquid state, at very high temperatures (>2500 °C), the miscibility gap is overcome and liquid Ag and Ni become soluble as shown in Fig. 9 (a). For this simple binary system, already 30 at.% of Ag dissolves in liquid Ni at 2500 °C [29]. The influence of W and C, which are also present in the system, on the actual solubility of Ag in the "eutectic" phase at high temperatures was thermodynamically calculated (Thermo-Calc 4.0 Software, Sweden) using the SGTE Solutions Database, Version 5.0 (SSOL5) which contains a critical assessment of the Ni–W–C ternary system [36]. A system identical to the overall composition of the "eutectic" phase (Table 2) was created in the software with the addition of up to 10 at.% Ag. Fig. 8 (a) shows that the volume fraction of the silver layer in the arc-affected zone is very low compared to that of the silver depleted layer. In spite of the high volume fraction of silver in the bulk, a very low amount of silver participates in this mechanism because most of the silver is lost by evaporation. Therefore, the Ni-rich region of the phase diagram is of primary interest. The dotted box in Fig. 9 (a) shows the region of interest without W and C. The calculated phase diagram is plotted in Fig. 9 (b) which shows that 4 at.% of Ag dissolves in liquid Ni at 2500 °C for a constant W (19 at.%) and C (13 at.%) content (Table 2).

4. Discussion

It is clear that the effect of Ni addition on the contact resistance is not proportional as one would expect from literature [13–15]. It is also not possible to correlate or predict the evolution of R_c with increasing Ni content from the hardness of the bulk composite. This is because of the microstructural changes and layer formation during switching. Once these persistent layers are formed, the

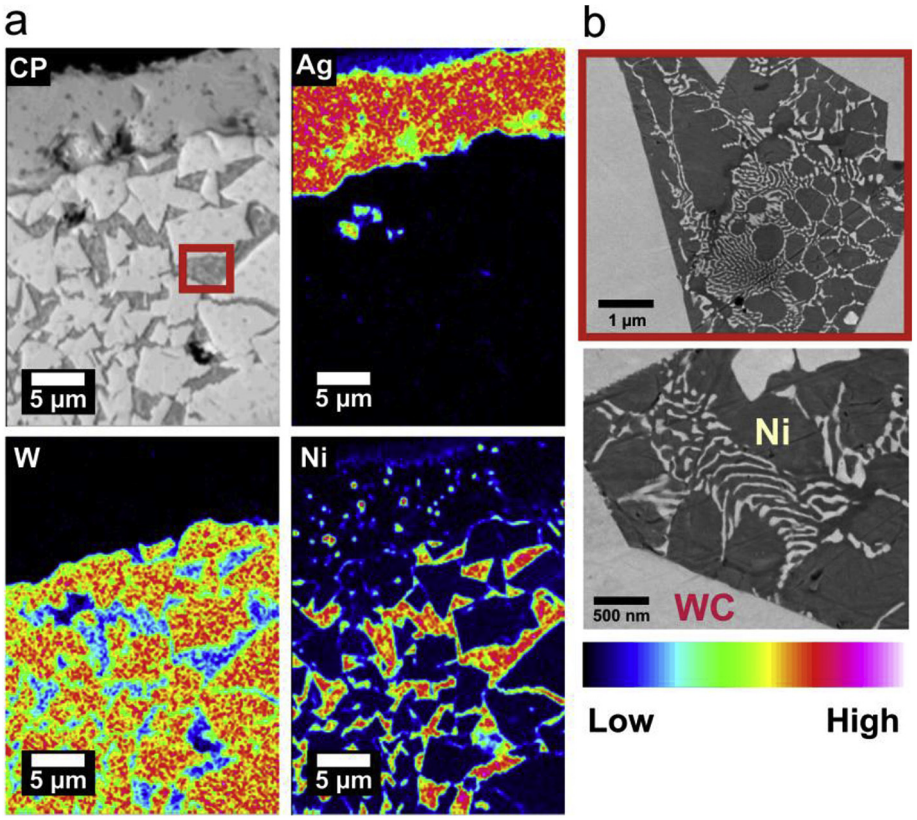

Fig. 6. (a) Elemental mapping of the Ni10Ag55 material after 50 switching cycles at higher magnification (of Fig. 5 (b)) showing the (i) Ag layer and (ii) Ag depleted layer; (b) Magnified back-scattered electron image of the selected box region in (a) showing the eutectic phase formed in the Ag depleted layer.

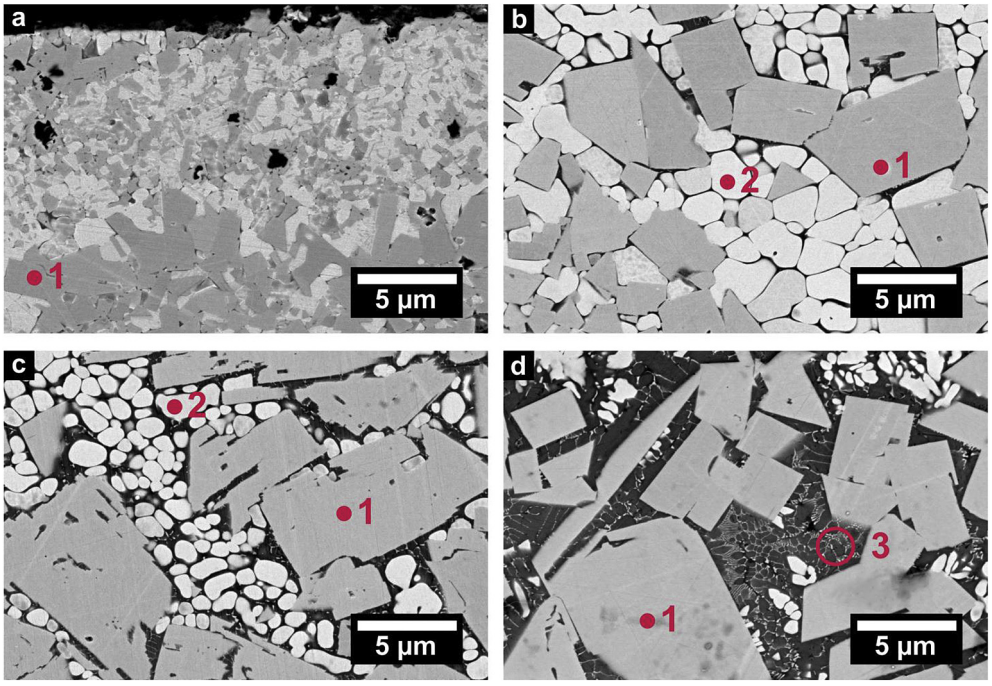

Fig. 7. Backscatted electron imaging showing the evolution of the silver depleted layer (region ii in Fig. 4 and Fig. 5) containing (a) 1, (b) 3, (c) 6.5 and (d) 10 wt.% of Ni.

physical, mechanical and electrical properties of the bulk material have minor influence on the R_c, which can only be measured after each switching cycle.

By combining the microstructure after switching with the predicted thermodynamic stability of all possible phases at high temperature, it is possible to explain the mechanism of silver

Table 2
Quantitative electron probe microanalysis of phase 1, 2 and 3 labelled in Fig. 7, representative for the three constituent phases present in the silver-depleted layer in region ii of Fig. 5 (b).

Element	Phase 1		Phase 2		Phase 3	
	wt.%	at.%	wt.%	at.%	wt.%	at.%
W	91.1 ± 0.3	49.7 ± 0.6	94.1 ± 0.6	68.5 ± 0.5	44.7 ± 0.9	18.9 ± 0.5
C	6.0 ± 0.1	50.3 ± 0.6	2.6 ± 0.1	28.4 ± 0.1	2.0 ± 0.1	13.1 ± 0.7
Ni	–	–	1.4 ± 0.3	3.2 ± 0.6	51.5 ± 0.3	68.0 ± 0.2

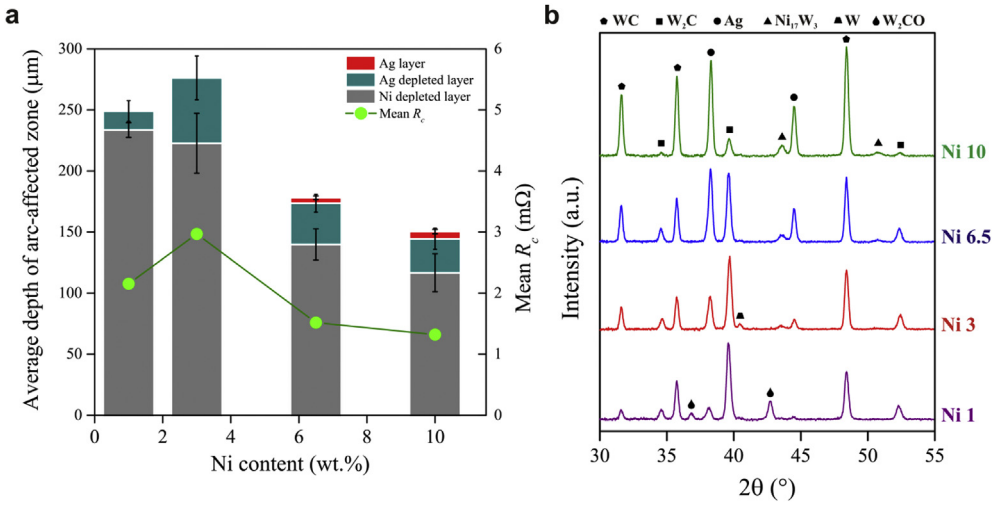

Fig. 8. (a) Average measured thickness of the layers present in the arc-affected zone for the different Ni containing contact materials, and the evolution of the average contact resistance as a function of the Ni content. (b) Representative XRD patterns of the investigated contact materials containing 1, 3, 6.5 and 10 wt.% of Ni after 50 switching cycles.

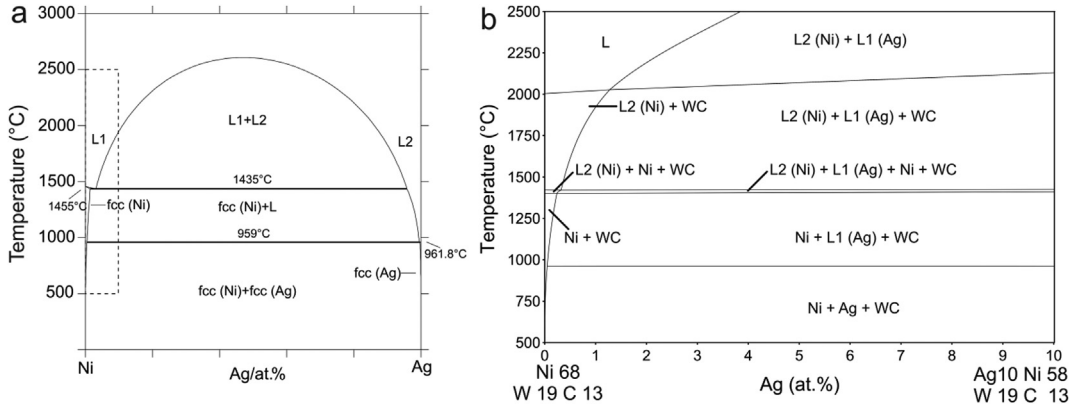

Fig. 9. (a) Ni–Ag binary phase diagram re-plotted from [29] showing the region of interest. (b) Calculated phase diagram (Thermo-Calc 4.0) showing the solubility of silver in the "eutectic" phase of the silver depleted layer at constant W and C content.

transport from the bulk of the material through the Ag-depleted layer towards the surface. When the electric-arc strikes the contact surface, the temperature of the contact rises rapidly with a steep gradient. At temperatures above 2700 °C, silver evaporates and ~4 at.% silver dissolves in the liquid phase (see Fig. 9 (b)). When the electric arc extinguishes, the contact starts to cool down from the base copper rod (heat sink) towards the contact surface. With a decrease in temperature, the solubility of liquid Ag in liquid Ni starts to decrease, leading to phase separation followed by solidification of Ni. The direction of solidification dictates that the Ni solidifies in the silver depleted layer (region ii in Fig. 5). This leads to a depletion of Ni in the region (iii) as most of the Ni from this layer was molten during the heating cycle and now is solidified in the region (ii). Simultaneously, the liquid Ag segregates out of the cooling melt and is pushed ahead of the solidification front forming the Ag-rich top layer on the contact. Although some silver is still soluble in the Ni-rich continuous phase of the eutectic in the solid state, with further decrease in temperature, the excess Ag eventually solidifies on top of the Ni-rich layer. This explains the formation of the silver-rich surface layer on top of the silver-depleted layer (Ni-rich layer), as found in the transverse section of the contacts (Fig. 5). The eutectic, WC-Ni phase acts as a buffer, which temporarily "stores" the silver at high temperatures and releases it on top due to directional solidification. Moreover, the amount of silver solidified on top is determined by the amount of eutectic phase present in the silver-depleted layer. At low Ni contents

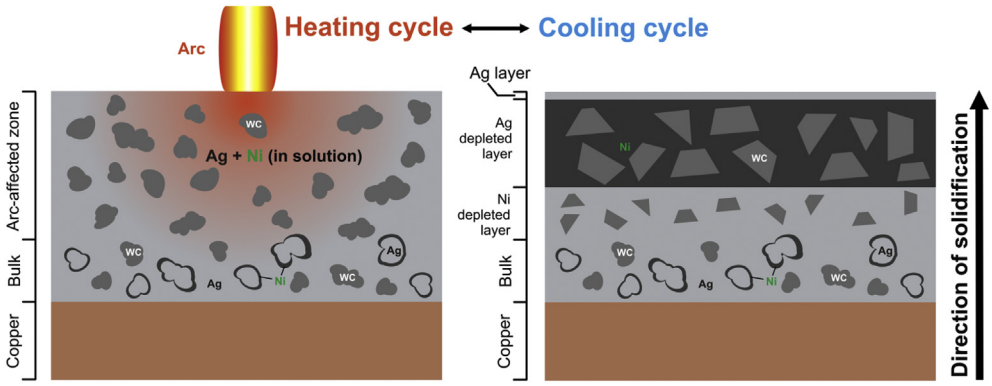

Fig. 10. Schematic illustration of the transportation of silver from the bulk to the contact surface during thermal cycling.

(~3 wt.%) the bright rounded grains are dominant (Phase 2 in Fig. 7) over the eutectic phase in the silver depleted layer, thus no silver layer is formed. Only when the Ni content is further increased, the volume fraction of eutectic phase increases and results in the formation of a silver layer. The R_c initially increases with increase in Ni content (~3 wt.%) due to the formation of a hard and brittle silver-depleted layer. However, with further increase in Ni amount, the soft silver layer is formed and the R_c drops abruptly. This phenomenon of transporting the silver from the bulk to the contact surface during the heating and cooling cycle is illustrated in Fig. 10.

5. Conclusion

Four Ag-WC-Ni metal matrix composites with increasing Ni content of 1, 3, 6.5 and 10 wt.% were prepared by liquid metal infiltration of a porous sintered body. These composites were further subjected to thermal cycling in a break-only model switching device for 50 operations at 50 Hz and peak current of 1300A. The average electrical contact resistance (R_c) measured across the contact pair during the 50 cycles increased from ~2 to ~3 mΩ with the amount of Ni increasing from 1 to 3 wt.% in the composite. With further increase in Ni content up to 10wt.%, the R_c started decreasing from ~3 to ~1.5 mΩ. The arc-affected zone after 50 cycles revealed a strong gradient in elemental composition which allowed classifying the arc-affected zone into three layers, namely a silver-rich layer, a silver-depleted layer and a nickel-depleted layer from the contact surface towards the bulk material. The different layers formed during cooling, were a consequence of directional solidification from the copper heat sink towards the contact surface. The formation of a silver layer was only observed in contacts containing 6–10 wt.% of Ni, which was in correspondence with the decrease in R_c. In these high Ni containing materials, a eutectic phase of WC and Ni was formed during cooling which released the dissolved silver on top of the contact surface due to the decrease in solubility of Ag in the melt.

Acknowledgements

The authors are thankful to Dr. Shuigen Huang and Andrea Gil Santos from the Department of Materials Engineering, KU Leuven for their help with the thermodynamic calculations. The authors gratefully acknowledge support from the Flemish government via the Hercules Foundation (project ZW09-09). The authors also greatly appreciate the help from Christian Hubrich from Technical Materials, Umicore for his assistance with the break-only model switching device.

References

[1] J. Jaćimović, L. Felberbaum, E. Giannini, J. Teyssier, Electro-mechanical properties of composite materials for high-current contact applications, J. Phys. D. Appl. Phys. 47 (2014) 125501, http://dx.doi.org/10.1088/0022-3727/47/12/125501.
[2] F. Findik, H. Uzun, Microstructure, hardness and electrical properties of silver-based refractory contact materials, Mater. Des. 24 (2003) 489–492, http://dx.doi.org/10.1016/S0261-3069(03)00125-0.
[3] T. Mützel, R. Niederreuther, Development of Contact Material Solutions for Low-Voltage Circuit Breaker Applications (2), in: 57th IEEE Holm Conference on Electrical Contacts, Minneapolis, USA, 2011, pp. 1–6, http://dx.doi.org/10.1109/HOLM.2011.6034790.
[4] T. Mützel, B. Kempf, Silver tungsten carbide contacts for circuit breaker applications, in: 60th IEEE Holm Conference on Electrical Contacts, New Orleans, USA, 2014, pp. 1–7, http://dx.doi.org/10.1109/HOLM.2014.7031059.
[5] C.-H. Leung, H. Kim, A Comparison of Ag/W,Ag/WC, and Ag/Mo Electrical Contacts, IEEE Trans. Compon., Hybrid. Manuf. Technol. 7 (1984) 69–75, http://dx.doi.org/10.1109/TCHMT.1984.1136333.
[6] P.C. Wingert, C.-H. Leung, The development of silver-based cadmium-free contact materials, IEEE Trans. Compon. Hybrid. Manuf. Technol. 12 (1989) 16–20, http://dx.doi.org/10.1109/33.19007.
[7] K. Kaliszuk, K. Frydman, D. Wojcik-Grzybek, W. Bucholc, E. Walczuk, P. Borkowski, Arc erosion tests and study of surface of Ag-WC contacts after arc switching operations, in: 60th IEEE Holm Conference on Electrical Contacts, Seattle, USA, 2004, pp. 75–82, http://dx.doi.org/10.1109/HOLM.2004.1353098.
[8] J. Shea, Erosion and resistance characteristics of AgW and AgC contacts at high current arcing in air, in: 44th IEEE Holm Conference on Electrical Contacts, Arlington, USA, 1998, pp. 287–291, http://dx.doi.org/10.1109/HOLM.1998.722457.
[9] M.B. Schulman, P.G. Slade, J.A. Bindas, Effective erosion rates for selected contact materials in low-voltage contactors, IEEE Transactions on Components, Packag. Manuf. Technol. Part A 18 (1995) 329–333, http://dx.doi.org/10.1109/95.390312.
[10] H. Yu, Y. Sun, M.T. Kesim, J. Harmon, J. Potter, S.P. Alpay, Surface Degradation of Ag/W Circuit Breaker Contacts During Standardized UL Testing, J. Mater. Eng. Perform. (2015) 1–12, http://dx.doi.org/10.1007/s11665-015-1647-2.
[11] C.-H. Leung, P.C. Wingert, Microstructure effects on dynamic welding of Ag/W contacts, IEEE Transactions on Components, Hybrid. Manuf. Technol. 11 (1988) 64–67, http://dx.doi.org/10.1109/33.2963.
[12] T. Bregel, W. Krauss-Vogt, R. Michal, K.E. Saeger, On the application of W/Cu materials in the fields of power engineering and plasma technology, IEEE Transactions on Components, Hybrid. Manuf. Technol. 14 (1991) 8–13, http://dx.doi.org/10.1109/33.76502.
[13] P.C. Wingert, The effects of nickel on the switching performance of silver-tungsten-based contacts, in: 39th IEEE Holm Conference on Electrical Contacts, Pittsburgh, USA, 1993, pp. 111–115, http://dx.doi.org/10.1109/HOLM.1993.489667.
[14] G.J. Witter, The effect of nickel additions on the performance of tungsten-silver materials, in: 11th International Conference on Electric Contact Phenomenon Berlin, Germany, 1982, pp. 351–355.
[15] Z. Aslanoğlu, Y. Karakaş, M.L. Öveçoğlu, B. Özkal, Effects of nickel addition on properties of Ag–W electrical contact materials, Powder Metall. 44 (2001) 77–81, http://dx.doi.org/10.1179/003258901666202.
[16] A. Qureshi, S. Azhar, N. Hussain, The effect of cobalt addition on sintering and microstructural behaviour of silver–tungsten (Ag–W) composite, J. Therm. Analysis Calorim. 99 (2009) 203–209, http://dx.doi.org/10.1007/s10973-009-0152-y.
[17] N. Ray, B. Kempf, T. Mützel, L. Froyen, K. Vanmeensel, J. Vleugels, Effect of WC particle size and Ag volume fraction on electrical contact resistance and thermal conductivity of Ag–WC contact materials, Mater. Des. 85 (2015)

412–422, http://dx.doi.org/10.1016/j.matdes.2015.07.006.
[18] S.E. Allen, E. Streicher, The effect of microstructure on the electrical performance of Ag-WC-C contact materials, in: 44th IEEE Holm Conference on Electrical Contacts, Arlington, USA, 1998, pp. 276–285, http://dx.doi.org/10.1109/HOLM.1998.722456.
[19] N.M. Hwang, Y.J. Park, D.-Y. Kim, D.Y. Yoon, Activated sintering of nickel-doped tungsten: approach by grain boundary structural transition, Scr. Mater. 42 (2000) 421–425, http://dx.doi.org/10.1016/S1359-6462(99)00344-9.
[20] C. Buchegger, W. Lengauer, J. Bernardi, J. Gruber, T. Ntaflos, F. Kiraly, Diffusion parameters of grain-growth inhibitors in WC based hardmetals with Co, Fe/Ni and Fe/Co/Ni binder alloys, Int. J. Refract. Met. Hard Mater 49 (2015) 67–74, http://dx.doi.org/10.1016/j.ijrmhm.2014.06.002.
[21] C.M. Fernandes, A.M.R. Senos, Cemented carbide phase diagrams: A review, Int, J. Refract. Met. Hard Mater 29 (2011) 405–418, http://dx.doi.org/10.1016/j.ijrmhm.2011.02.004.
[22] G.S. Upadhyaya, Materials science of cemented carbides—an overview, Mater. Des. 22 (2001) 483–489.
[23] R.C. Hula, C. Edtmaier, M. Holzweber, H. Hutter, C. Eisenmenger-Sittner, The wetting behaviour of silver on carbon, pure and carburized nickel, cobalt and molybdenum substrates, Appl. Surf. Sci. 256 (2010) 4697–4701, http://dx.doi.org/10.1016/j.apsusc.2010.02.075.
[24] G.J. Witter, Electrical Contact Material and Method for Making the Same, 1979. US4162160 A.
[25] U.L. 489 Molded-case Circuit Breakers, Molded-case Switches, and Circuit Breaker Enclosures, ninth ed., 1996.
[26] P.C. Wingert, Testing of the thermal-stress-cracking characteristics of silver-refractory contacts, 41st IEEE Holm Conference on Electrical Contacts, Montreal, Canada, 1995, pp. 338–345. doi:10.1109/HOLM.1995.482889.
[27] G. Witter, W. Warke, A Correlation of Material Toughness, Thermal Shock Resistance, and Microstructure of High Tungsten, Silver-Tungsten Composite Materials, IEEE Trans. Parts, Hybrid. Packag. 11 (1975) 21–29, http://dx.doi.org/10.1109/TPHP.1975.1135028.
[28] F. Pons, M. Cherkaoui, An Electrical Arc Erosion Model Valid for High Current: Vaporization and Splash Erosion, in: 54th IEEE Holm Conference on Electrical Contacts, Orlando, USA, 2008, pp. 9–14, http://dx.doi.org/10.1109/HOLM.2008.ECP.15.
[29] X.J. Liu, F. Gao, C.P. Wang, K. Ishida, Thermodynamic Assessments of the Ag-Ni Binary and Ag-Cu-Ni Ternary Systems, J. Electron. Mater 37 (2007) 210–217, http://dx.doi.org/10.1007/s11664-007-0315-1.
[30] C. Wu, D. Yi, W. Weng, S. Li, J. Zhou, F. Zheng, Arc erosion behavior of Ag/Ni electrical contact materials, Mater. Des. 85 (2015) 511–519, http://dx.doi.org/10.1016/j.matdes.2015.06.142.
[31] V.K. Gupta, D.-H. Yoon, H.M. Meyer III, J. Luo, Thin intergranular films and solid-state activated sintering in nickel-doped tungsten, Acta Mater. 55 (2007) 3131–3142, http://dx.doi.org/10.1016/j.actamat.2007.01.017.
[32] M.H. de Sá, I. Isomäki, J.A. Ferreira, M. Hämäläinen, M.H. Braga, Experimental and First Principles Study of the Ni-Ti-W System, Mater. Sci. Forum 730–732 (2012) 775–780. 10.4028/www.scientific.net/MSF.730-732.775.
[33] M.S. Bazarjani, M.M. Müller, H.-J. Kleebe, C. Fasel, R. Riedel, A. Gurlo, In situ formation of tungsten oxycarbide, tungsten carbide and tungsten nitride nanoparticles in micro- and mesoporous polymer-derived ceramics, J. Mater. Chem. A 2 (2014) 10454–10464, http://dx.doi.org/10.1039/C4TA01509F.
[34] H. Okamoto, Ni-w (nickel-tungsten), J. Phase Equilib. 12 (1991), http://dx.doi.org/10.1007/BF02645185, 706–706.
[35] P. Franke, D. Neuschütz, S.G.T.E. (sgte), Ni-W, in: P. Franke, D. Neuschütz (Eds.), Binary Systems. Part 4: Binary Systems from Mn-mo to Y-zr, Springer Berlin Heidelberg, 2006, pp. 1–3.
[36] D.P. Gustafson, A. Gabriel, I. Ansara, Trita-mac 0263, 1985, p. 1986.